Elaboration and characterization of a free standing LiSICON membrane for aqueous lithium-air battery

Laurent Puech, Christophe Cantau, Philippe Vinatier, Gwenaëlle Toussaint, Philippe Stevens

Elaboration and Characterization of a Free Standing LiSICON Membrane for Aqueous Lithium-Air Battery

Laurent Puech[a,*], Christophe Cantau[a], Philippe Vinatier[a], Gwenaëlle Toussaint[b], Philippe Stevens[b]

[a] *CNRS, Université de Bordeaux, ICMCB site de l'ENSCBP-IPB, 87 avenue du Dr. A. Schweitzer, Pessac, F-33608, France*
Phone number: +33540006993; Fax number: +33540006698
[b] *EDF R&D, Moret-sur-Loing, France*

Abstract

In order to develop a LISICON separator for an aqueous lithium-air battery, a thin membrane was prepared by a tape-casting of a $Li_{1.3}Al_{0.3}Ti_{1.7}(PO_4)_3 - AlPO_4$ based slip followed by a sintering step. By optimizing the grain sizes, the slip composition and the sintering treatment, the mechanical properties were improved and the membrane was reduced to a thickness of down to 40 µm. As a result, the ionic resistance is relatively low, around 38 Ω for a 55 µm membrane of 1 cm^2. One side of the membrane was coated with a lithium oxynitrured phosphorous (LiPON) thin film to prevent lithium metal attack. Lithium metal was electrochemically deposited on the LiPON surface from a saturated aqueous solution of LiOH. However, the ionic resistance of the LiPON film, around 67 Ω for a 1.2 µm film of 1 cm^2, still causes an important ohmic loss contribution which limits the power performance of a lithium-air battery.

Keywords: Metal-air battery, Lithium anode, $Li_2O - Al_2O_3 - TiO_2 - P_2O_5$ system, LiPON, Solid electrolyte

1. Introduction

Metal-air batteries are based on the use of a metal negative electrode in combination with an oxygen positive electrode. Such a positive electrode theoretically has an infinite capacity, because the active material –the oxygen gas– is not stored in the battery, only the product of the reaction is. Among the different metals, lithium is very interesting because of its high theoretical capacity (around 3 800 Ah/kg) and the favourable oxydo-reduction potential of the Li^+/Li couple versus these of the oxygen: $\Delta E = 3.4$ V for aqueous oxygen electrodes and $\Delta E = 3.0$ V for non-aqueous oxygen electrodes. As a result, lithium-air batteries have a high theoretical energy density at more than 10 000 Wh/kg, comparable to that of gasoline (13 000 Wh/kg). However, this density is only related to the mass of lithium and does not include the other components of the battery: the air electrode, its discharge product, the liquid and solid electrolytes and the package. Moreover, the practical useable energy density and the power density of the battery are limited by the ohmic loss caused essentially by the electrical resistance of the solid electrolytes. As a result, an energy density of 500 Wh/kg may be considered to be a more realistic but still very interesting objective.

The first rechargeable lithium-air battery was made by Abraham and Jiang [1] in 1996. It consisted of a Li metal foil as anode, an organic polymer membrane as solid electrolyte and a thin carbon composite exposed to pure oxygen as the oxygen electrode. Such a battery based on non-aqueous electrolyte is generally limited by the formation of Li_2O_2 inside the pores of the oxygen electrode and by the decomposition of the organic solvent resulting from the formation to a super-oxide radical [2]. Aqueous lithium-air batteries using an aqueous electrolyte such as LiOH solution do not have these problems. The product of the reaction ($LiOH,H_2O$) is stored as a solid in the aqueous compartment and not in the electrode [3]. Moreover, the use of a polymeric anion-exchange membrane in the oxygen electrode prevents LiOH precipitation inside the electrode, but also the formation of Li_2CO_3. Such a cathode can run with untreated air. Among the other main limitations, the oxygen electrode has a poor reversibility. It can be destroyed by the oxygen evolution during the charge of the battery. Toussaint *et al.* [4] proposed an oxygen bi-electrode: during the charge, a stainless steel electrode in the aqueous electrolyte shunts the porous air electrode to play the role of an oxygen evolution electrode.

A watertight protection of the lithium electrode is however necessary to prevent its oxidation by the water. This protective barrier needs to be stable to the aqueous electrolyte. Aono *et al.* [5] proposed a water-stable NaSICON-like electrolyte: $Li_{1+x}Al_xTi_{2-x}(PO_4)_3$ (LATP). For $x \sim 0.3$, this LiSICON offers a good ionic conductivity, close to 7×10^{-4} S/cm. Thokchom and Kumar [6] proposed a way to elaborate a membrane based on $14Li_2O - 9Al_2O_3 - 38TiO_2 - 39P_2O_5$ (LATP-AP), a composite of LATP and $AlPO_4$. This stoichiometry was chosen by these authors because of the reproducibility of its synthesis and its good

*Corresponding author: puech@icmcb-bordeaux.cnrs.fr; Phone number: +33540006993; Fax number: +33540006698.

ionic conductivity, similar to that of LATP. The solid electrolyte should also be protected from attack by lithium metal. This can be done using a lithium-stable electrolyte as a lithium oxynitrured phosphorous glass (LiPON) as proposed by Bates *et al.* [7]. This can be obtained as a thin film by the sputtering of a Li_3PO_4 target under a nitrogen discharge. Its low thickness compensates its relative low ionic conductivity, close to 2×10^{-6} S/cm. Alternatively, a liquid organic electrolyte such as 1 M $LiClO_4$ in ethylene carbonate/dimethyl carbonate can be used between the LiSICON membrane and the lithium metal as proposed by Wang *et al.* [8]. The liquid acts as an interface between the lithium and the LiSICON, but the formation of lithium dendrites will eventually come in contact with and attack the ceramic electrolyte to destroy it. A very good electrode/electrolyte interface can also be obtained by using a stainless steel thin film (0.3 µm) as current collector, coated onto the LiPON thin film protection [9]: the lithium metal is then electrochemically deposited between the LiPON and the current collector from a saturated lithine solution during first charge process after the battery manufacture.

In a previous study [3], an aqueous lithium-air battery was made using an oxygen bi-electrode (see figure 1). On the anode side, the solid electrolyte consisted to a glass-ceramic LiSICON membrane supplied by Ohara [10] coated by a protective LiPON film. As descripted above, the lithium electrode was electrochemically deposited after the battery manufacture. However, the thickness of the Ohara membrane (160 µm) was still too high and induced a resistance of around 160 Ω for one cm^2 area. Such a resistance causes an important ohmic loss which limits the performances of the battery.

The aim of this work was to improve the lithium half-cell with a thinner membrane, less than 50 µm, and based on a ceramic LATP-AP powder, chosen for the reproducibility of its synthesis and its high conductivity. This membrane should be sufficiently strong to be free standing and to be manipulated. The lithium half-cell built with this membrane was then characterized by electrochemical analyses by depositing a lithium electrode and evaluated.

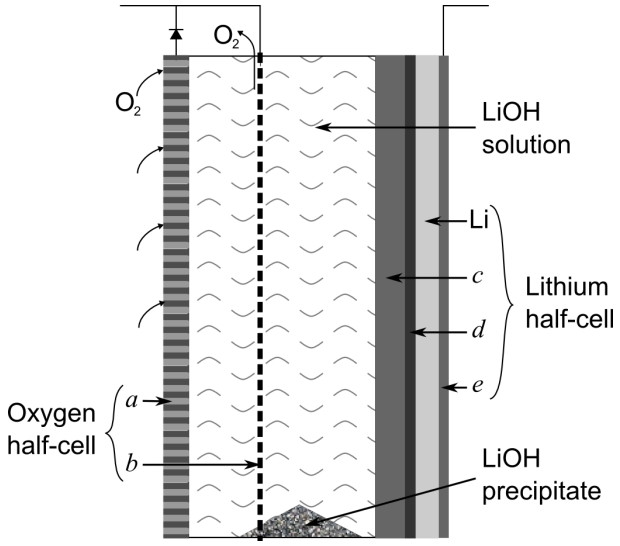

Figure 1: Aqueous lithium-air battery as proposed by P. Stevens *et al.* [3]. *a*: O_2 reduction electrode with a polymeric anion-exchange membrane; *b*: O_2 evolution electrode (stainless steel grid); *c*: LiSICON membrane; *d*: protective LiPON thin film; *e*: stainless steel current collector (thin film); Li film: electrochemically deposited after the battery manufacture.

2. Experimental

2.1. Synthesis of LATP-AP Powder and its Characterizations

As proposed by Thokchom and Kumar [6], a LATP-AP glass was prepared by melting a Li_2CO_3, Al_2O_3, TiO_2 and $NH_4H_2PO_4$ mixture at 1450°C followed by tempering on a steel plate heated close to 500°C. The glass was then milled by planetary ball milling to obtain a powder. The LATP-AP glass was crystallised by heating at 900°C for 10 hours. In order to obtain submicronic and homogeneous grain size powder, attrition milling was performed during 5 hours using ethanol as a solvent.

Thermal dilatometric analyses were done using a Netzsch 402ED dilatometer. These consisted in measuring variations in the length of pellets with the furnace temperature using a saphir reference. The thermal treatment constituted in heating at 10°C/min from room temperature to 1200°C, followed by cooling of the furnace to room temperature.

The X-ray diffraction analyses were performed using a Philips X'Pert Powder diffractometer equipped with a Cu anode ($\lambda = 1.5418$ Å).

2.2. Elaboration of the Lithium Half-Cell

A ceramic LATP-AP powder based slip was made with ethanol and xylene as solvents, menhaden oil as dispersant, benzyl-butyl phtalate (BBP) and poly-ethylene glycol (PEG) as plasticizers, and poly(vinyl-butyral-co-vinyl-alcohol-co-vinyl-acetate) (PVB-VA-VAc) as binder. The slip composition needs to be adjusted to optimize its rheological properties depending on the grain size of the ceramic powder and to improve the mechanical properties of the membrane before and after the sintering.

A raw membrane was prepared by a tape casting of the slip with a thickness of 0.15 mm on a silicone coated Mylar sheet. After the elimination of the solvents at room temperature, this membrane was peeled off and disposed between two silica glass plates to conserve its flatness. The organic additives were eliminated during a slow heating step (+0.25°C/min) followed by a 1 hour plateau at 450°C. The membrane was then sintered with a rapid heating rate (+7.2°C/min) and a 1 hour plateau at 1080°C.

For the LiPON deposit, a Li_3PO_4 target was made from milled β-Li_3PO_4 powder. In order to avoid that the $\beta \rightarrow \gamma$ phase transition at 500°C occurs during the sintering step, the powder was heated at 850°C during 12 hours.

Film	LiPON	SSCC
Thickness	1.6 µm	0.3 µm
Target	Li_3PO_4	Stainless steel
Gas	N_2	Ar
Flow	45 SCCM	50 SCCM
Pressure	1.0 Pa	1.0 Pa
Power	40 W	50 W
Duration	8 hours	20 minutes

Table 1: Parameters of the thin film deposition; SSCC: stainless steel current collector; SCCM: cm^3/min at 25°C and 1 bar.

A γ-Li_3PO_4 based pellet was prepared with a 5 cm diameter and a 4 mm thickness, and sintered at 620°C during 12 hours. The target was then glued onto a copper backing plate using a silver epoxy glue.

LiPON and the stainless steel current collector (SSCC) thin films were deposited by RF magnetron sputtering using a Plassys MP 300 T apparatus opening in a dry box under argon with the parameters listed on the table 1. In the two cases, the pressure was kept during the deposition at 1 Pa using a Vat vacuum valve and a Vat PM-3 pressure controller.

The negative compartment was then built under normal laboratory air.

2.3. Impedance Measurements and Electrochemical Analyses

Two SSCC thin films were deposited by RF magnetron sputtering on the two side of a 56 µm LATP-AP membrane. Impedance measurements were performed using a Solartron 1260 impedance analyser, with a 10 mV amplitude and a frequency varying between 1 Hz and 10 MHz. In order to measure the impedance of a 0.75 µm LiPON film, a SSCC/LiPON/SSCC sandwich structure was deposited by RF magnetron sputtering on a glass substrate with an overlap area of 0.04 cm^2. Impedance measurements were performed with a 50 mV amplitude and using the same impedance analyser and the same frequency range as those of LATP-AP.

To evaluate its performances during the charge process, the lithium half-cell was disposed vertically in contact with an aqueous 2 M LiOH solution and a stainless steel counter electrode. The working electrode potential was measured using a Hg/HgO/KOH (1 M) reference electrode. The cyclic voltammogram was performed using a Biologic VMP3 potentiostat at a scan rate of 20 mV/s between −0.5 and −3.5 V versus Hg/HgO/KOH (1 M).

3. Results and Discussion

3.1. Synthesis of the LATP-AP membrane

After treating the glassy LATP-AP powder at 900°C for 10 hours, the X-ray diffractrogram is typical of a crystallized sample (see figure 2). As a result, we can consider this powder to be a ceramic powder elaborated from

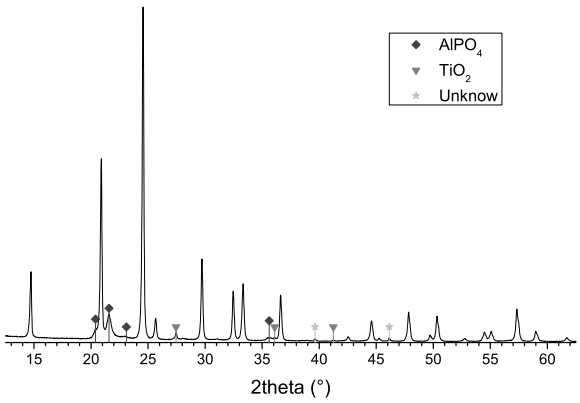

Figure 2: X-ray diffractrograms of the synthesized ceramic LATP-AP powder; unmarked peaks are attributed to $Li_{1.3}Al_{0.3}Ti_{1.7}(PO_4)_3$.

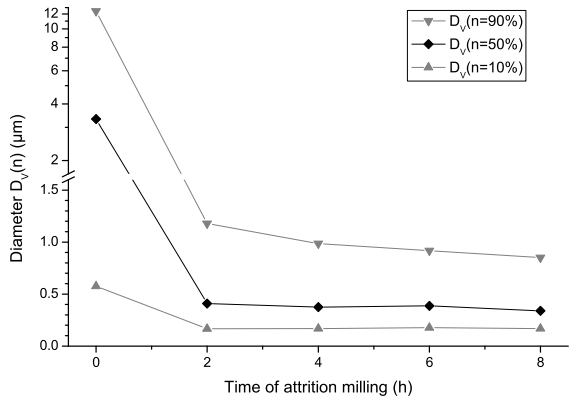

Figure 3: Plot of the grain diameter $D_V(n)$ versus the time of attrition milling, according to the laser granulometry; n is the volume ratio of the grains which are smaller than $D_V(n)$.

a glass-ceramic process. As proposed by Wong *et al.* [11], the most intensive peaks can be identified as a NASICON-like structure: $LiTi_2(PO_4)_3$ (LTP) [12] with a change of the cell volume. The constants a and c can be estimate to 8.501 Å and 20.82 Å respectively, instead of 8.513 Å and 20.878 Å for LTP. These values are very closed to those determined by Aono *et al.* [5] for $Li_{1+x}Al_xTi_{2-x}(PO_4)_3$ with $x \sim 0.3$. Because of the aluminium substitution, the cell volume decreases: the Al^{3+} radius (0.535 Å) is inferior than the Ti^{4+} radius (0.605 Å). According to Wong *et al.* [11], other peaks can be attributed to $AlPO_4$ and rutile (TiO_2). These results are in accordance with the composition of LATP-AP: $14Li_2O - 9Al_2O_3 - 38TiO_2 - 39P_2O_5$ may correspond to $Li_{1.3}Al_{0.3}Ti_{1.7}(PO_4)_3 - (\sim 0.5)\,AlPO_4 - (\sim 0.06)\,TiO_2$. Beside these structures, two peaks, 39.64° and 46.12°, are unattributed.

The laser granulometry results varying with the duration of the attrition milling (see figure 3) show drastic decreases of both the median grain size $D_V(50\%)$, close to 0.4 µm after 2 hours, and the diameters $D_V(10\%)$ and

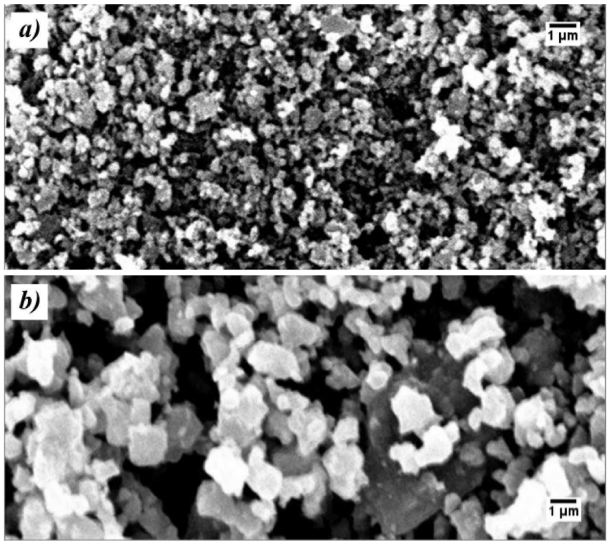

Figure 4: Ceramic LATP-AP powder after *(a)* and before *(b)* the attrition milling by SEM.

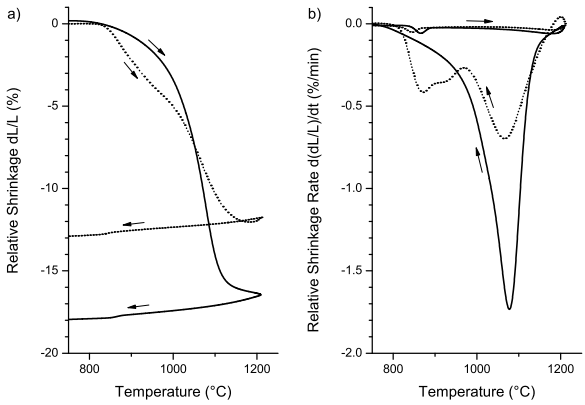

Figure 5: Thermal dilatometric analyses of ceramic LATP-AP before *(dotted lines)* and after *(solid lines)* the attrition milling; the arrows indicate temperature evolutions versus time: increasing until 1200°C then decreasing.

Nature	Constituent	Mass ratio
Ceramic	LATP-AP	58.5%
Solvents	Ethanol	18.1%
	Xylene	15.8%
Dispersant	Menhaden oil	1.1%
Plasticizers	BBP	1.1%
	PEG	1.1%
Binder	PVB-VA-VAc	4.3%

Table 2: Optimized slip composition.

$D_V(90\%)$ –the diameter $D_V(n)$ is the maximal size of the smallest grains constituting the volume ratio n of the powder. These decreases are also visible by scanning electron microscopy (see figure 4). Moreover, we can note an improvement of the homogeneity of the grain sizes: the ratio of $D_V(90\%)$ versus $D_V(10\%)$ decreases from up to 20 to near 5 after a 5 hours attrition milling.

Optimization of the sintering is an important key to improve the density and to obtain a strong and efficient membrane. To evaluate effects of optimized milling on the sintering, thermal dilatometric analyses of ceramic LATP-AP powder were performed before and after the attrition milling. We notice a higher shrinkage for the milled powder (see figure 5a). Before the attrition milling, according to the shrinkage rate curve (see figure 5b), the sintering is broken down into three steps corresponding to the three local maximums of the rate: 870°C, 915°C and 1065°C. This may be the consequence of the heterogeneity of the grain sizes. After a five hours attrition milling, the shrinkage rate curve only presents a peak at 1080°C. This is coherent with the improvement of the grains size homogeneity. Moreover, this analysis enabled us to define the optimal temperature of sintering at 1080°C for a maximal shrinkage. This helped us to reduce the membrane thickness without losing its mechanical properties.

Because of the increase in the powder specific surface, the slip constituents and their concentrations needs be adapted: the solvents proportions should be increased to keep the rheological properties of the slip. Moreover, it is necessary to increase the binder ratio to facilitate the removal of the raw membrane from the Mylar sheet. However, too high proportion of organic additives may cause kracks during the sintering. The proposed slip composition (see table 2) improved the mechanical properties of the raw membrane and helped us to reduce its thickness, and also kept its cohesion after the sintering.

As a result, we obtained a free standing and handleable membrane (see figure 6). Its thickness is closed to 40 µm according to the section measurement by SEM (see figure 7). Its density is estimated to be around 2.8 g/cm^3 by buoyancy measurements into diethylphtalate and water. This value is close to the LATP-AP theoretical density, between 2.7 and 2.8 g/cm^3. However, as volume loss induced by open pores is not taken account by buoyancy measurements, we can estimate that the compactness is below one. We notice the presence of pores on the cross-section views (see figure 7b), which probably results from the gas evolution during the elimination of the organic constituents. Inside the pores, the grains have a cushion-like shape, whereas on the fracture, its have a more angular shape resulting from the optimized sintering.

3.2. Impedance Measurements

Impedance measurements were performed on a ceramic LATP-AP membrane (see figure 8). Its electrical behaviour is modelled by a parallel circuit consisting of a resistance R_{LATP} and a constant phase element $\mathrm{CPE}_{\mathrm{LATP}}$. As proposed among others by Hamon *et al.* [13], a serial resistance R_{S1} and a serial constant phase element CPE_{S1} should be use to model the electrical behaviour of the

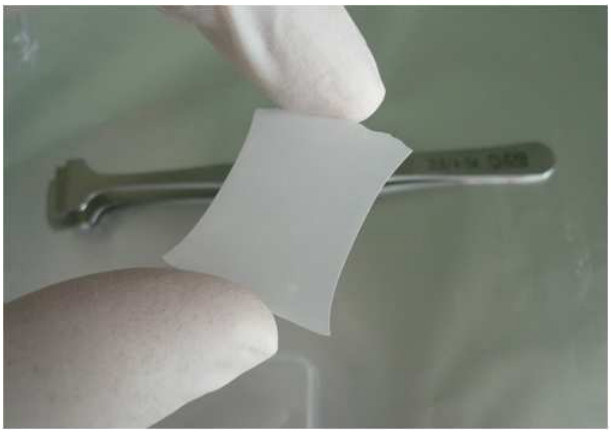

Figure 6: Resulting free standing LATP-AP membrane.

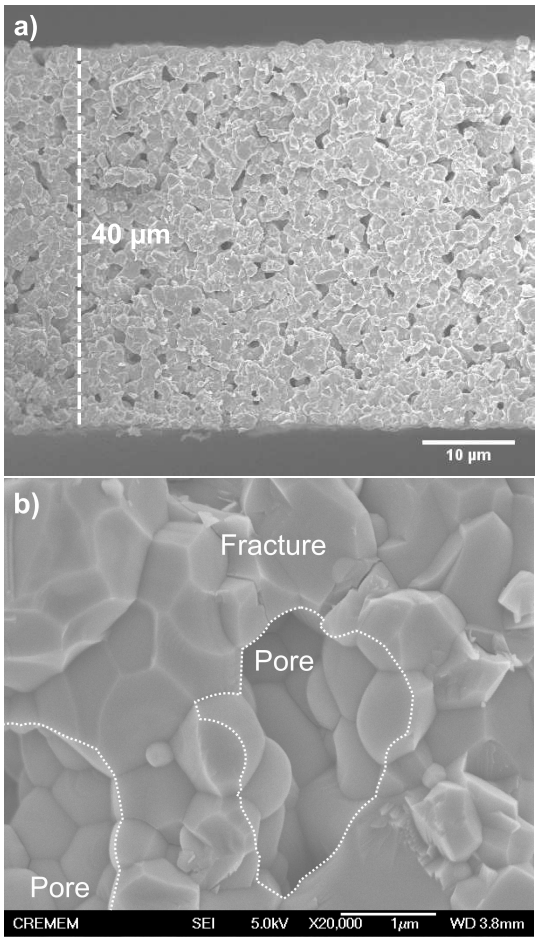

Figure 7: Cross-section of LATP-AP membrane by SEM.

a)

LATP circuit		**Serial circuit**	
R_{LATP} (Ω)	39	R_{S1} (Ω)	7.2
Q_{LATP} (F)	2.5×10^{-7}	Q_{S1} (F)	1.6×10^{-6}
P_{LATP}	0.87	P_{S1}	0.92

b)

LiPON circuit		**Serial circuit**	
R_{LiPON} (Ω)	1820	R_{S2} (Ω)	260
Q_{LiPON} (F)	8.1×10^{-9}	Q_{S2} (F)	3.0×10^{-6}
P_{LiPON}	0.85	P_{S2}	0.91

Table 3: Equivalent circuit parameters of the LATP-AP membrane (a) and the LiPON thin film (b) at 298 K.

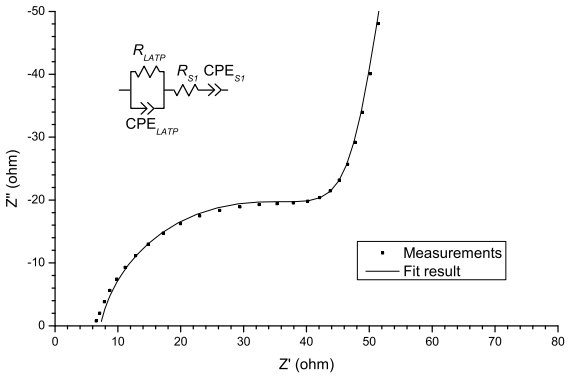

Figure 8: Cole-cole plot of LATP-AP membrane and its equivalent electrical circuit.

stainless steel electrodes. R_{S1} accounts for the current collector resistance and a CPE is used because the current collector is not a perfectly blocking electrode. The CPE impedance Z_{CPE} is a function of a capacity Q and a potency P ($0 < P < 1$):

$$Z_{\mathrm{CPE}} = \frac{1}{Q\,(i\omega)^{P}} \tag{1}$$

As a result, the impedance Z_{LATP} of the equivalent circuit is expressed by:

$$Z_{\mathrm{LATP}} = \frac{1}{\frac{1}{R_{\mathrm{LATP}}} + Q_{\mathrm{LATP}}\,(i\omega)^{P_{\mathrm{LATP}}}} + R_{S1} + \frac{1}{Q_{S1}\,(i\omega)^{P_{S1}}} \tag{2}$$

The ohmic resistance of the LATP-AP membrane can be identified with R_{LATP}. As a result, the determination of equivalent circuit parameters (see table 3) enabled us to estimate the ionic conductivity of the membrane at 1.8×10^{-4} S/cm.

Similar impedance measurements were performed on a LiPON film (see figure 9). According to previous studies including those of Hamon *et al.* [13], the impedance

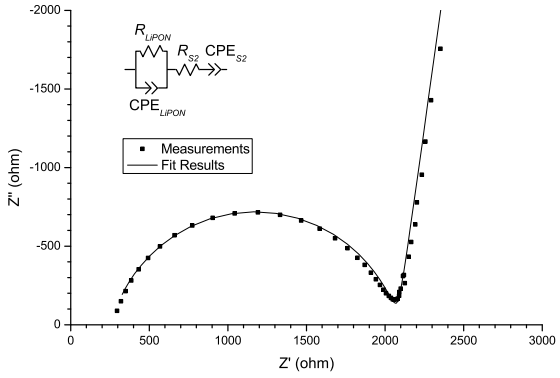

Figure 9: Cole-cole plot of LiPON thin film at 298 K and its equivalent electrical circuit.

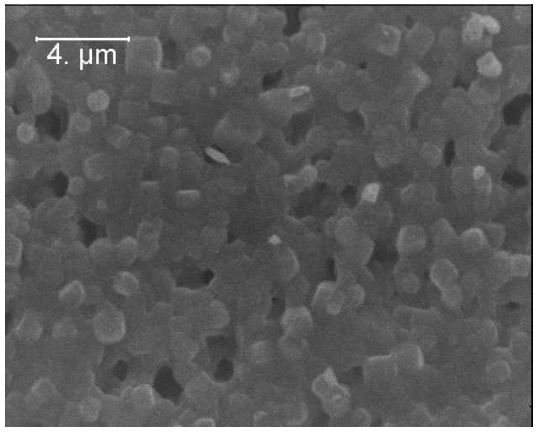

Figure 11: Surface of sintered LATP-AP membrane by SEM.

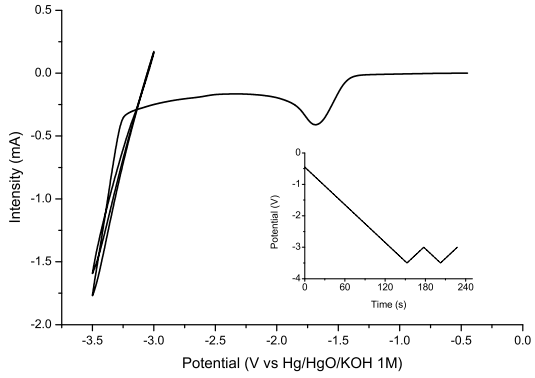

Figure 10: Measured intensity versus working electrode potential. *Inset:* Applied working electrode potential during the cyclic voltammetry. Main cyclic voltammetry parameters: 20 mV/s scan rate, 0.42 cm^2 electrode surface, 2 M LiOH aqueous solution.

Z_{LiPON} can be expressed by:

$$Z_{\mathrm{LiPON}} = \frac{1}{\frac{1}{R_{\mathrm{LiPON}}} + Q_{\mathrm{LiPON}} (i\omega)^{P_{\mathrm{LiPON}}}} + R_{S2} + \frac{1}{Q_{S2} (i\omega)^{P_{S2}}} \quad (3)$$

As above, the resistance of the LiPON film can be identified with R_{LiPON}. We calculated the ionic conductivity to be close to 1.8×10^{-6} S/cm at 298 K using the equivalent circuit parameters (see table 3).

3.3. Electrochemical Analyses

A gradually increasing reduction potential E_{we} was applied on the working electrode of the half-cell and measured with a Hg/HgO/KOH (1 M) reference electrode, up to −3.5 V (see figure 10). Between −1.5 and −1.9 V, the local current peaks are probably due to the electrochemical reduction of impurities as adsorbed water. This artefact produced low currents which suggested that these impurities was present in low quantities: they did not seem to have destructive effect on the half-cell. Once the reduction potential of Li^+ is reached at −3.3 V, a rapid increase in current is observed due to the lithium metal electroplating. When reversing the cycle by decreasing the applied potential between −3.5 V and −3.0 V, the electrochemically deposited lithium metal is consumed by electrochemical oxidation of lithium metal to Li^+. Between −3.0 V and −3.5 V, the cyclic voltametry curve presents a straight shape which corresponds to a reversible phenomenon. We can estimate a resistance close to 105 Ω for one cm^2 area from the slope of this straight curve. If we calculate the membrane ohmic resistance by the addition of the resistance of a 55 µm LATP-AP membrane, 38 Ω.cm^2, and the resistance of a 1.2 µm LiPON thin film, 67 Ω.cm^2, we obtain the same value. This demonstrates that the electrochemical lithium metal deposition during charge and the lithium consumption during discharge are limited only by the lithium ion conduction through the solid electrolyte. As a result, we can conclude that the interface resistances are negligible compared to the membrane resistance. The absence of a large water reduction peak in the voltamogram also shows that the LATP-AP membrane appears to be watertight.

3.4. Discussion about the protective coating

We can note that the LiPON resistance, 67 Ω for a one cm^2 area of a 1.2 µm film, contributes for a large part to the total membrane resistance, as a result of its low conductivity (1.8×10^{-6} S/cm). On the surface of the membrane (see figure 11), we can observe pores with a size close to 1 µm. As a consequence, a LiPON film of more than 1 µm is necessary to compensate for the membrane roughness. This is caused by the micron size grains which constitute 10% in volume according to the measurement of the grain size distribution (see figure 3) and by the evolution during the elimination of the organic additives.

One solution to reduce the LiPON thickness would be to reduce the roughness of the ceramic membrane. This could be done by the elaboration of a membrane using

smaller grains. Instead of a solid state reaction followed by a milling step, some authors [14, 15] mentioned the possibility to synthesizing smaller LATP grains by using soft chemistry processes: this route enabled Wu *et al.* [16] to elaborate micronic LATP film.

An other solution could be to replace the LiPON film by a lithium-stable Li^+ ionic conductor. Xu *et al.* [17] reported on the good stability of the interface between $Li_{1.5}Al_{0.5}Ge_{1.5}(PO_4)_3$– 0.05 Li_2O and a lithium metal anode. Moreover, this ceramic had a higher conductivity than LiPON, around 5×10^{-3} S/cm according to Thokchom *et al.* [18]. However, the interface with a lithium anode introduced an important ohmic loss, around 20 kΩ, according to impedance plots from Xu *et al.* [17] and our own studies. Deiseroth *et al.* [19] presented Li-argyrodite materials, Li_6PS_5X (X ≡ Cl or Br), with a conductivity close to 10^{-3} S/cm. Moreover, Stadler and Fietzek [20] announced that this material have good stability in contact with lithium anode. Recently, a new lithium superionic conductor, $Li_{10}GeP_2S_{12}$, was reported by Kanno *et al.* [21] with a conductivity higher than 10^{-2} S/cm and a good electrochemical stability front of a lithium anode.

4. Conclusion

An optimized milling, an optimized slip composition and an optimized sintering enabled us to prepare a ceramic LATP-AP membrane which was sufficiently strong to be free standing and handleable. This membrane was sufficiently thin to minimize its ionic resistance and therefore significantly reduced the ohmic loss in an aqueous lithium-air cell. Moreover, electrochemical analyses in contact with an aqueous solution showed that this membrane was watertight. Finally, growth of lithium from an aqueous solution was demonstrated in a lithium half-cell using a thin LATP-AP membrane. However, this study pointed out the limiting effect of the protective LiPON thin film, with an ionic resistance higher than that of the LATP-AP membrane. As a result, for a current density of 10 $mAh.cm^{-2}$, a 1 V ohmic loss through the membrane can be estimated. This value is too high to reach a good energy density and power density. Further studies should be performed to reduce the LiPON thickness, for example by reducing the roughness of the membrane surface, or to substitute the LiPON by a better ionic conductor. This study of a thin LiSICON membrane was an important step to demonstrate the feasibility of an aqueous lithium-air battery and to solve its main limitations.

Acknowledgement

The authors acknowledge financial support provided by the french national agency for research (ANR) under the STOCK-E program, LIO and LIO2 project.

[1] K. M. Abraham, Z. Jiang, J. Electrochem. Soc. 143 (1) (1996) 1–5.
[2] C. O. Laoire, S. Mukerjee, K. M. Abraham, E. J. Plichta, M. A. Hendrickson, J. Phys. Chem. C 113 (46) (2009) 20127–20134.
[3] P. Stevens, G. Toussaint, G. Caillon, P. Viaud, P. Vinatier, C. Cantau, O. Fichet, C. Sarrazin, M. Mallouki, Electrochem. Soc. Trans. 28 (32) (2010) 1–12.
[4] G. Toussaint, P. Stevens, L. Akrour, R. Rouget, F. Fourgeot, Electrochem. Soc. Trans. 28 (32) (2010) 25–34.
[5] H. Aono, E. Sugimoto, Y. Sadaoka, N. Imanaka, G.-Y. Adachi, J. Electrochem. Soc. 136 (2) (1989) 590–591.
[6] J. S. Thokchom, B. Kumar, J. Electrochem. Soc. 154 (4) (2007) A331–A336.
[7] J. B. Bates, N. J. Dudney, G. R. Gruzalski, R. A. Zuhr, A. Choudhury, C. F. Luck, Solid State Ionics 53-56 (1992) 647–654.
[8] Y. Wang, H. Zhou, J. Power Sources 195 (2010) 358–361.
[9] G. Toussaint, P. Stevens, G. Caillon, P. Viaud, C. Cantau, P. Vinatier, patent n° FR2950737 (A1) (2011).
[10] http://www.ohara-inc.co.jp/en/product/electronics/licgc.html.
[11] S. Wong, P. J. Newman, A. S. Best, K. M. Nairn, D. R. MacFarlane, M. Forsyth, J. Mater. Chem. 8 (10) (1998) 2199–2203.
[12] Natl. Bur. Stand. (U.S.) Monogr. 25 21 (1985) 79.
[13] Y. Hamon, A. Douard, F. Sabary, C. Marcel, P. Vinatier, B. Pecquenard, A. Levasseur, Solid State Ionics 177 (2006) 257–261.
[14] Y. Ando, N. Hirose, J. Kuwano, M. Kato, H. Otsuka, Ceram. Today-Tomorrow's Ceram. (1991) 2242–2252.
[15] M. Cretin, P. Fabry, L. Abello, J. Eur. Ceram. Soc. 15 (1995) 1149–1156.
[16] X. M. Wu, X. H. Li, S. W. Wang, Z. Wang, Y. H. Zhang, M. F. Xu, Z. Q. He, Thin Solid Films 425 (2003) 103–107.
[17] X. Xu, Z. Wen, X. Wu, X. Yang, Z. Gu, J. Am. Ceram. Soc. 90 (9) (2007) 2802–2806.
[18] J. S. Thokchom, N. Gupta, B. Kumar, J. Electrochem. Soc. 155 (12) (2008) A915–A920.
[19] H.-J. Deiseroth, S.-T. Kong, H. Eckert, J. Vannahme, C. Reiner, T. Zaiß, M. Schlosser, Angew. Chem. Int. Ed. 47 (2008) 755–758.
[20] F. Stadler, C. Fietzek, Electrochem. Soc. Trans. 25 (32) (2010) 177–183.
[21] N. Kamaya, K. Homma, Y. Yamakawa, M. Hirayama, R. Kanno, M. Yonemura, T. Kamiyama, Y. Kato, S. Hama, K. Kawamoto, A. Mitsui, Nat. Mater. 10 (9) (2011) 682–686.